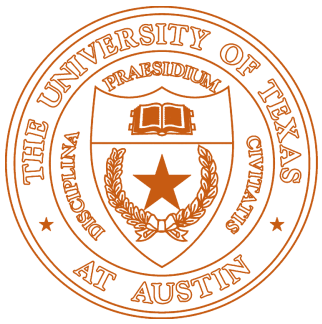

The University of Texas at Austin

Honors Thesis in Physics

Negative Index Metamaterials for Particle Acceleration and Radiation Generation

---

Author:
William Frierson

Research Adviser:
Dr. Gennady Shvets

Signature:

May 7, 2010

Negative Index Metamaterials for Particle Acceleration and Radiation Generation

May 7, 2010

Abstract

Metamaterials (MTMs) are engineered materials with remarkable applications. They unnaturally bend light via their intricate structures, rather than through some novel substance or chemical composition. MTMs are being used to develop, *e.g.*, a 'superlens' (which has an optical resolution exceeding the theoretical limit) and a cloaking device (which effectively makes an object invisible by bending light around it). We investigated a MTM made by stacking parallel metal sheets, which have a periodic pattern called the complementary split-ring resonator (CSRR). Our computational models show how the CSRR MTM can accelerate charged particles and generate terahertz radiation (1 THz = 10^{12} Hz).

Using numerical methods from COMSOL software, we simulated how the CSRR manipulates microwave light. The program looks for the CSRR's resonant frequencies of light and their corresponding oscillations (called modes). We first confirmed previous results from Dr. Michael Shapiro at MIT, then continued to characterize the electrodynamic properties of the CSRR MTM. The CSRR MTM has one accelerating mode, which exists at frequencies between 5.34 GHz and 5.65 GHz (1 GHz = 10^9 Hz). The accelerating mode has a negative refractive index (NRI), where refractive index is a quantity based on the electric and magnetic properties of a material. MTMs are the only known materials possessing a NRI. We demonstrated the mode's NRI by approximating the CSRR as a periodic circuit, and extracted critical electrodynamic information. Finally, we examined how the CSRR MTM interacts with an electron beam, by simulating them simultaneously. We observed 'electron bunching,' which is a key property for the CSRR MTM's applications.

The accelerating mode pushes and focuses charged particles along one axis. Effectively, the accelerating mode 'kicks' the particles in one direction, and ensures they stay in a line. This action is highly desired for particle acceleration. Lastly, the CSRR MTM may be used to develop terahertz radiation devices, namely coupled-cavity traveling-wave tubes. Terahertz radiation generators are anticipated to usher in myriad advances in medical imaging, spectroscopy, and technology.

Introduction

Metamaterials is new a branch of optics research, which is concerned with the manipulation of light. Because of physicists like Maxwell and Huygens, optics is well understood. The set of equations which describes light, called Maxwell's equations, indicates how materials bend light. In particular, a material's magnetic and electric characteristics entirely describe how it interacts with light. These quantities are called 'magnetic permeability,' μ, and 'electric permittivity,' ϵ. Permeability and permittivity are used to determine a material's refractive index, n, by,

$$n = \sqrt{\mu\epsilon}. \tag{1}$$

In practice, refractive index is mostly used in determining how light interacts with materials.

Although most materials have positive μ and ϵ, acheiving a negative ϵ is not difficult. Many metals, such as gold, have a negative ϵ for visible light. In fact, this is why we cannot see through metals. However, all natural materials which are transparent have positive μ and ϵ. In 1968, Victor Veselago theorized a material with both negative μ and ϵ[1]. He showed that such an exotic material would give a real refractive index (rather than complex), which means light can propogate through it. Strangely, this material would have a negative refractive index, which yields very peculiar properties. Most notably, light would bend in the 'wrong' direction, as seen in Fig. 1. Also, forward traveling light would appear to oscillate backwards, as if ocean waves hitting the shore seemed to ripple *towards* the sea.

This MTM property is called 'backwards wave propagation,' and is observed via a MTM's dispersion. Dispersion is a common phenomenon in optics, where the frequency of light, f, depends on its wavevector, $\mathbf{k} = (kx, ky, kx)$, where $k_i = \frac{2\pi}{\lambda}$ and λ is the wavelength of light in the i-direction. Natural materials have a positive slope when plotting f vs. $\mathbf{k}$, *i.e.*, $\frac{df}{d\mathbf{k}} > 0$. However, MTMs have a negative slope, $\frac{df}{d\mathbf{k}} < 0$.

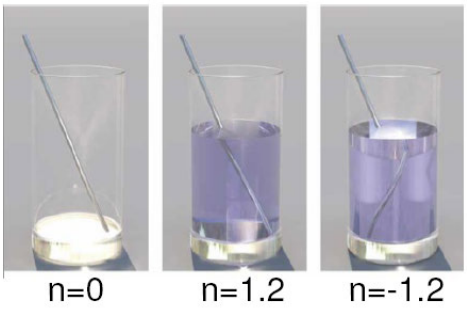

Figure 1: Simulations comparing how light bends in different refractive indices, n[2]

Veselago's hypothetical material was not widely investigated, until 1999 when John Pendry et al.[3] proposed methods to make an artificial negative index material, or metamaterial. Shortly after, David Smith et al.[4] created another MTM, called a split-ring resonator (SRR), based on Pendry's original concept. In general, MTMs are repeating patterns made of metal, or a combination of metal and dielectric. The pattern arrangement is as important as the pattern itself. For example, a planar pattern MTM has different properties than a vertically stacked pattern MTM, even if the pattern is the same in each MTM. *Thus, MTM properties mostly arise from its internal and external geometry* – the pattern used and the pattern arrangement, respectively. Currently, numerous MTM designs have been found (See Fig. 2).

Despite the various designs, MTM properties originate from a similar mechanism. Suppose light is directed toward a MTM, and its magnetic field strikes a particular cell of a MTM (*i.e.*, one of the metallic patterns). The electrons in the metal form a characteristic current[5], which is a complex function of the pattern's geometry and the incoming light's energy. From this current, the MTM cell generates its own magnetic field, which induces similar current in a neighboring cell. This process continues, and so incident light creates a characteristic current which propagates through the entire MTM (see Fig. 3).

Since the interesting MTM effects come from the electrodynamic properties of each MTM cell, we need methods to observe them. Experimentalists construct a particular MTM, and determine,

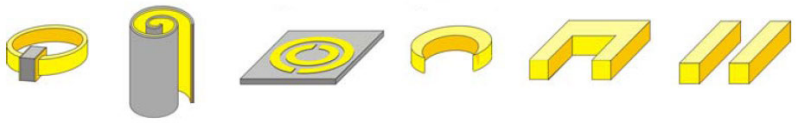

(a) Various metamaterial patterns(5)

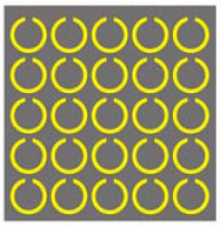

(b) Metamaterials are repeating patterns of metal, or metal and dielectric.(5)

(c) Split-ring resonator (SRR) pattern(4)

Figure 2: Examples of metamaterials

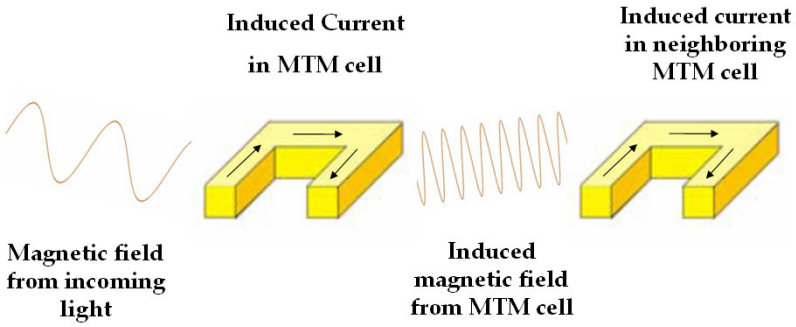

Figure 3: Metamaterial properties come from the surface currents generated by incoming light

e.g., its NRI and induced electromagnetic fields. Theoretical and computational physicists typically simulate a MTM instead. Simulations tend to be much cheaper, and are easier to manipulate. This paper involves only theoretical and computational models of MTMs.

To simulate the interactions of light with a MTM, we need Maxwell's equations, which are a set of partial differential equations relating magnetic (**H**) and electric fields (**E**):

$$\begin{aligned} \nabla \cdot \mathbf{E} &= \frac{\rho}{\epsilon_0} \\ \nabla \cdot \mathbf{H} &= 0 \\ \nabla \times \mathbf{E} &= -\mu_0 \frac{\partial \mathbf{H}}{\partial t} \\ \nabla \times \mathbf{H} &= \mathbf{J} + \epsilon_0 \frac{\partial \mathbf{E}}{\partial t}, \end{aligned} \tag{2}$$

where ρ is charge density, $\mathbf{J}$ is current density, & ϵ_0 and μ_0 are the respective permittivity and permeability in vacuum. Maxwell's equations represent the laws which propagating light must obey

in a medium. Solutions to Maxwell's equations give the electric and magnetic fields which describe light. Because MTMs have complex geometries, we cannot analytically solve Maxwell's equations. Instead, we use the finite element method (FEM), which approximates the solution to Maxwell's equations.

FEM numerically solves partial differential equations (PDEs) by dividing a model into a finite number of sections (called elements). Classical methods for solving PDEs assume the geometry is continuous, *i.e.*, the PDE must be solved at the infinitely many points along the geometry. When the geometry is complex, analytic solutions are essentially impossible. FEM avoids this problem by solving the PDE at the intersections of elements, called nodes.

For the CSRR MTM, we used commercial FEM software, called COMSOL. Exactly how COMSOL solves Maxwell's equations is discussed in the theory section. In short, Maxwell's equations are reduced to one equation involving only the electric field. We provide a fixed wavevector $\mathbf{k}$ and a guess at the electric field's frequency f. COMSOL then searches for electric fields in the MTM which have such a wavevector and frequency. Once the electric field is found, the magnetic field is calculated using Maxwell's equations. $\mathbf{E}$ and $\mathbf{H}$ are then used to calculate all other electrodynamic quantities.

To show a computational model is a MTM, we require its effective μ and ϵ to be simulatenously negative. Unfortunately, there are no classical methods for calculating μ and ϵ. However in 2002, Eleftheriades et al.[6] suggested an approximate solution by modeling MTMs as transmission lines. A transmission line (TL) is a material used to direct energy, and is modeled as a periodic circuit. The circuit is described by a function of impedance, Z, and admittance, Y (which are two circuit parameters). The energy flowing through the TL is described by voltage and current. Input voltage and current are transformed as they pass through the unit cell of the periodic circuit (See Fig. 4). The output voltage and current are calculated from the transmission (ABCD) matrix, which depends on the placement of Z and Y in the periodic circuit (See Eq. (3)).

$$\begin{bmatrix} V_{in} \\ I_{in} \end{bmatrix} = \begin{bmatrix} A & B \\ C & D \end{bmatrix} \begin{bmatrix} V_{out} \\ I_{out} \end{bmatrix} \tag{3}$$

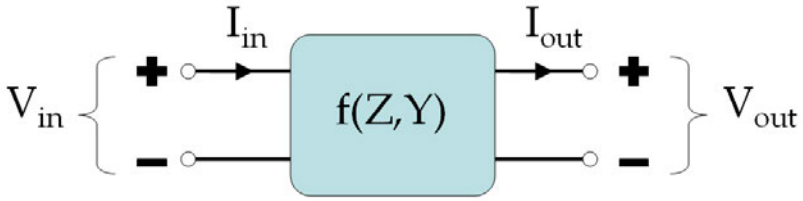

Figure 4: The unit cell of a periodic circuit, which models a transmission line.

TLs are most compactly described by the telegrapher's equations, which is a system of differential equations involving current, voltage, Z, and Y. For certain types of light, Eleftheriades showed *μ and ϵ are proportional to Z and Y* (resp.), by corresponding the telegrapher's equations for TLs with Maxwell's equations. Thus, when Z and Y are simultaneously negative, so are μ and ϵ – the material has a NRI.

As outlined in the theory section, we computed Z and Y for the CSRR MTM using two perdiodic circuits: a symmetric and an asymmetric circuit. From each circuit's transmission matrix, we derived equations for Z and Y in terms of simulated $\mathbf{E}$ and $\mathbf{H}$ fields. Most of these equations were motivated by Dr. Michael Shapiro of MIT.

The dimensions of the CSRR pattern are shown in Table 1. The cell dimensions are $b = 8$ mm in the x- and y-directions, and $d = 12.8$ mm in the z-direction. The thickness of the metal sheet is $t = 0.05$ mm. We simulated the CSRR MTM using one cell (See Fig. 5). To model the MTM as an infinite plane, we made the boundaries periodic, and set an x-direction phase difference $\phi_x = kx\ x$ between cells. The y-direction had a zero degree phase advance, and the z-boundaries had settings dependent on the calculation performed.

Width	8 mm
Outer ring slot length	6.6 mm
Slot width	0.8 mm
Split width	0.3 mm
Thickness	0.05 mm

Table 1: CSRR dimensions

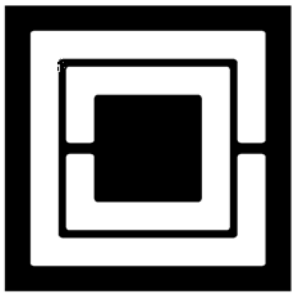

Figure 5: The unit cell of the complementary split-ring resonator metamaterial (CSRR MTM).

As its name implies, complementary split-ring resonators are the counterparts to split-ring resonators. In general, 'complementary materials' switch the metal and vacuum with respect to the parent material (Compare Figs. 2c and 5). Pendry[3] showed that SRRs have resonant permeability, which means μ becomes negative when incident light is near a characteristic frequency. The Babinet principle[7] relates electrodynamic properties between a material and its complement. In particular, the Babinet principle shows the CSRR has resonant permittivity[8], and so it becomes negative for certain frequencies of incident light. The Babinet principle also indicates that electric fields primarily excite CSRRs. This electric coupling is the critical mechanism for our applications: particle acceleration and generating radiation.

The CSRR MTM is actually a waveguide, which is an engineering device used to direct electromagnetic energy. Our results show the CSRR MTM has an accelerating mode, which has a longitudinal electric field parallel to the planar CSRR sheet (which we call the x-direction). In addition, this mode has a NRI. Since electric fields apply a force to charged particles, this mode can accelerate charged particles along the x-axis (See Fig. 6). To excite the accelerating mode, we must send light between the metal sheets, which has the resonant frequency of the mode. Thus, we can increase an electron beam's energy by pumping light which excites the accelerating mode.

We also propose that the CSRR MTM can extract energy from an electron beam – effectively reversing particle acceleration. This mechanism is similar to a coupled-cavity traveling-wave tube. In this device, 'slow wave' light decelerates an electron beam. As the beam slows down, its lost energy is converted into radiation, through the coupling between the beam and the light. Thus, our CSRR MTM can act as a radiation source, by sending an electron beam in the negative direction

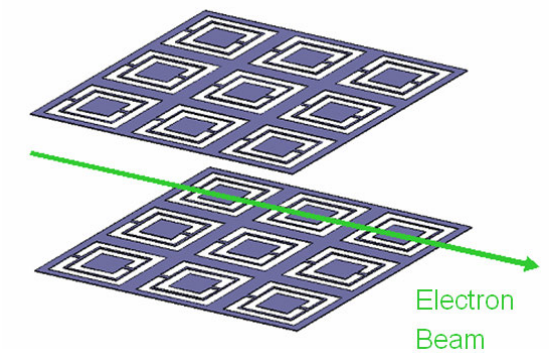

Figure 6: Electron beam accelerating in the CSRR MTM waveguide.[9]

(See Fig. 7). By scaling down the CSRR's dimensions, we theoretically can generate THz radiation. Because of physical limitations, THz radiation has largely been unexplored. With its numerous applications, THz radiation devices will be a critical, technological advancement.

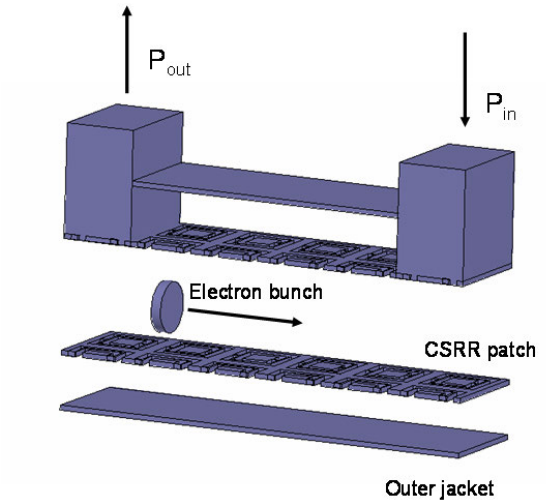

Figure 7: The CSRR MTM can be used to accelerate an electron beam (via sending resonant light through P_{in}) or generate radiation (via extracting beam energy through P_{out}).[9]

Theory

Finite Element Method (FEM)

COMSOL solves Maxwell's equations using FEM via the Galerkin method. In the Galerkin method, a continuous problem is converted into a 'weak form' which is solved over finitely many points of the domain. First, a variational expression (called a functional) is defined from the governing PDE. The minimum of the functional gives an approximate solution to Maxwell's equations. The Galerkin method discretizes the functional's minimum, in order to create a solvable linear system. To derive the weak form of Maxwell's equations, we first assume time-harmonic solutions (using the engineering sign convention):

$$\begin{aligned}\mathbf{E} &= \mathbf{E}_0 e^{i\omega t} \\ \mathbf{H} &= \mathbf{H}_0 e^{i\omega t} \\ \mathbf{J} &= \mathbf{J}_0 e^{i\omega t}.\end{aligned} \tag{4}$$

Now if we examine $\nabla \times \nabla \times \mathbf{E}$, we have,

$$\begin{aligned}\nabla \times \nabla \times \mathbf{E} &= \nabla \times \left(-\mu_0 \frac{d\mathbf{H}}{dt}\right) \\ &= \nabla \times (-i\omega\mu_0 \mathbf{H}) \\ &= -i\omega\mu_0 \nabla \times \mathbf{H} \\ &= -\mu_0 \left(i\omega \mathbf{J} - \epsilon_0 \omega^2 \mathbf{E}\right) \\ &= \frac{\omega^2}{c^2}\mathbf{E} - i\omega\mu_0 \mathbf{J}.\end{aligned} \tag{5}$$

From Eq. (5), we define the functional[10],

$$F(\mathbf{E}) \equiv \int dV \ \left(\nabla \times \nabla \times \mathbf{E} - \frac{\omega^2}{c^2}\mathbf{E} + i\omega\mu_0 \mathbf{J}\right) \cdot \mathbf{E} \tag{6}$$

In order to minimize F, we desire $\mathbf{E}$ such that $\delta F(\mathbf{E}) = 0$, where,

$$\delta F(\mathbf{E}) \equiv \int dV \ \left(\nabla \times \nabla \times \mathbf{E} - \frac{\omega^2}{c^2}\mathbf{E} + i\omega\mu_0 \mathbf{J}\right) \cdot \delta\mathbf{E}, \tag{7}$$

where $\delta\mathbf{E}$ is an arbitrary function satisfying the boundary conditions of $\mathbf{E}$. We simplify $\delta F(\mathbf{E})$ as follows.

Using the vector identity,

$$\mathbf{A} \cdot (\nabla \times \mathbf{B}) = \mathbf{B} \cdot (\nabla \times \mathbf{A}) - \nabla \cdot (\mathbf{A} \times \mathbf{B}), \tag{8}$$

we set $\mathbf{A} = \delta\mathbf{E}$ and $\mathbf{B} = \nabla \times \mathbf{E}$:

$$(\nabla \times \nabla \times \mathbf{E}) \cdot \delta\mathbf{E} = (\nabla \times \mathbf{E}) \cdot (\nabla \times \delta\mathbf{E}) - \nabla \cdot (\delta\mathbf{E} \times (\nabla \times \mathbf{E})) \tag{9}$$

Applying the Divergence Theorem and vector triple product, Eqns. (7) and (9) imply,

$$\begin{aligned}\delta F(\mathbf{E}) = \int dV \ &\left((\nabla \times \mathbf{E}) \cdot (\nabla \times \delta\mathbf{E}) - \frac{\omega^2}{c^2}\mathbf{E} \cdot \delta\mathbf{E} + i\omega\mu_0 \mathbf{J} \cdot \delta\mathbf{E}\right) \\ &+ \oint dS \ \delta\mathbf{E} \cdot (\mathbf{n} \times (\nabla \times \mathbf{E})),\end{aligned} \tag{10}$$

From Eq. (10), we define the weak form of Maxwell's equations:

$$\boxed{\text{Weak Form} \ \equiv \ (\nabla \times \mathbf{E}) \cdot (\nabla \times \delta\mathbf{E}) - \frac{\omega^2}{c^2}\mathbf{E} \cdot \delta\mathbf{E} + i\omega\mu_0 \mathbf{J} \cdot \delta\mathbf{E}.} \tag{11}$$

This definition implies the flux integral in Eq. (10) is zero,

$$
\begin{aligned}
0 = & \oint dS\ \delta\mathbf{E} \cdot (\mathbf{n} \times (\nabla \times \mathbf{E})) \\
= & \oint dS\ \delta\mathbf{E} \cdot (\mathbf{n} \times (-i\omega\mu_0 \mathbf{H}))\,,
\end{aligned}
\tag{12}
$$

which implies (on the boundary),

$$
\mathbf{n} \times \mathbf{H} = 0. \tag{13}
$$

This is called the *natural boundary condition* of the weak form, and implies boundaries behave as perfect magnetic conductors (PMCs). If we started with $\mathbf{H}$ instead, the natural boundary conditions require the boundaries to be perfect electric conductors (PECs). COMSOL then transforms the weak form into a linear system.

Between adjacent CSRR patterns, we introduce a phase advance ϕ_x along the x-direction, where $\phi_x = kx\ x$. This is called Floquet periodic boundary conditions. The phase advance in the y-direction is zero degrees. We adjust the vertical boundary conditions for a desired calculation. COMSOL then solves for $\mathbf{E}$ and ω, through standard eigenvalue algorithms.

Corresponding Maxwell's and the Telegrapher's Equations

We now outline Eleftheriades' derivation for modeling a MTM as a distributed network[6]. The 2D telegrapher's equations representing the distributed network shown in Fig. 8 are,

$$
\begin{aligned}
\frac{\partial V_z}{\partial x} + \frac{\partial V_z}{\partial y} = & -Z(I_x + I_y) \\
\frac{\partial I_x}{\partial x} + \frac{\partial I_y}{\partial y} = & -YV_z
\end{aligned}
\tag{14}
$$

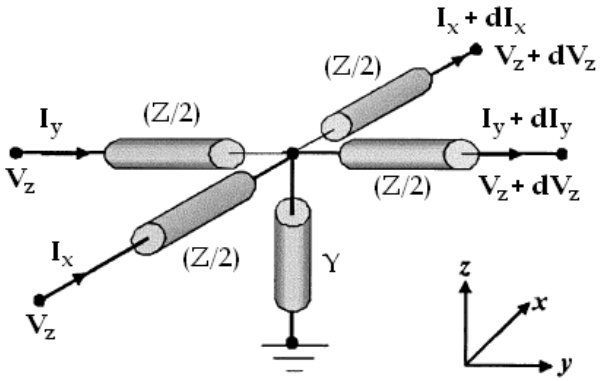

Figure 8: The unit cell of a 2D distributed network[6].

We now consider a mode with weak z-variation, such as a TM_z mode. This assumption implies $\frac{\partial}{\partial z} \approx 0$. Motivated from the definitions of voltage and Ampere's law, we relate Maxwell's and the telegrapher's equations by setting,

$$
\begin{aligned}
V_z &= E_z, \\
I_x &= H_y, \\
I_y &= -H_x.
\end{aligned}
\tag{15}
$$

Thus the telegrapher's equations imply (with $\mathbf{J} = 0$),

$$\begin{aligned} -YV_z &= \frac{\partial I_y}{\partial y} + \frac{\partial I_x}{\partial x} \\ &= \frac{\partial H_y}{\partial x} - \frac{\partial H_x}{\partial y} \\ &= -i\omega\epsilon E_z \qquad \text{(using the physics sign convention)} \\ &= -i\omega\epsilon V_z, \end{aligned} \tag{16}$$

and

$$\begin{aligned} -Z(I_x + I_y) &= \frac{\partial V_z}{\partial x} + \frac{\partial V_z}{\partial y} \\ &= \frac{\partial E_z}{\partial x} + \frac{\partial E_z}{\partial y} \\ &= \left(\frac{\partial E_x}{\partial z} - i\omega\mu H_y\right) + \left(\frac{\partial E_y}{\partial z} + i\omega\mu H_x\right) \\ &\approx (-i\omega\mu H_y) + (i\omega\mu H_x) \\ &= -i\omega\mu(I_x + I_y). \end{aligned} \tag{17}$$

Thus we obtain,

$$\boxed{\begin{aligned} Y &= i\omega\epsilon \\ Z &= i\omega\mu. \end{aligned}} \tag{18}$$

Z and Y Derivation using Symmetric Circuit

Both Drs. Shvets and Shapiro modeled the CSRR MTM as a 1D TL using a symmetric circuit (See Fig. 9). Although the CSRR MTM is a quasi-3D photonic crystal, its applications are easily modeled as 1D systems. Thus, we used the 1D telegrapher's equations:

$$\begin{aligned} \frac{\partial V}{\partial x} &= -ZI \\ \frac{\partial I}{\partial x} &= -YV. \end{aligned} \tag{19}$$

Approximating Eq. (19) using finite difference, we solve for Z and Y:

$$\boxed{\begin{aligned} Z &= -\frac{\Delta V}{\Delta x}\frac{1}{I} \\ Y &= -\frac{\Delta I}{\Delta x}\frac{1}{V}, \end{aligned}} \tag{20}$$

where $\Delta x = b$.

We define V and I by computing them at one edge, and phase shift them to the center of the cell with $e^{-i\frac{\phi x}{2}}$:

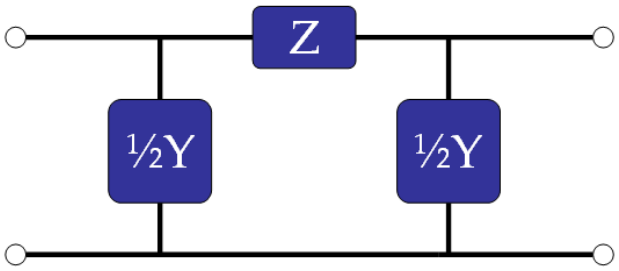

Figure 9: The unit cell of a 1D symmetric circuit.

$$\boxed{\begin{aligned} I &\equiv e^{-i\frac{\phi_x}{2}} \int dy \;\; H_y|_{x=-\frac{b}{2},\; z=\frac{t}{2}} \\ V &\equiv \frac{e^{-i\frac{\phi_x}{2}}}{b} \int dy \int dz \;\; E_z|_{x=-\frac{b}{2}}\,, \end{aligned}} \tag{21}$$

where all x and y bounds range from $-\frac{b}{2}$ to $\frac{b}{2}$, with z bounds from $\frac{t}{2}$ to $\frac{d}{2}$. I is motivated from part of an Amperian loop along the metal, and V is the average voltage at $x=-\frac{b}{2}$.

ΔV and ΔI are motivated from Maxwell's equations (assuming a TM_y mode $\Rightarrow \frac{\partial}{\partial y} \approx 0$). For ΔI, consider (using the engineering sign convention),

$$\begin{gathered} \frac{\partial H_y}{\partial x} = i\omega\epsilon_0 E_z \\ \Downarrow \\ \int dy \;\; \left(H_y|_{x=\frac{b}{2}} - H_y|_{x=-\frac{b}{2}}\right)\Big|_{z=\frac{t}{2}} = i\omega\epsilon_0 \int dx \int dy \;\; E_z|_{z=\frac{t}{2}}\,. \end{gathered} \tag{22}$$

The lefthand side of Eq. (22) is similar to a difference in currents. Thus, we define,

$$\boxed{\Delta I \equiv \; -i\omega\epsilon_0 \int dx \;\; \int dy \;\; E_z|_{z=\frac{t}{2}}\,.} \tag{23}$$

For ΔV, we also want a term which looks like a difference in voltages. Upon integrating $\frac{\partial E_z}{\partial x} = \frac{\partial E_x}{\partial z} + i\omega\mu_0 H_y$, we have,

$$\begin{aligned} \frac{1}{b}\int dy \int dz \;\; \left(E_z|_{x=\frac{b}{2}} - \; E_z|_{x=-\frac{b}{2}}\right) &= \frac{i\omega\mu_0}{b}\int dV \;\; H_y \\ &+ \frac{1}{b}\int dx \int dy \;\; \left(E_x|_{z=\frac{d}{2}} - E_x|_{z=\frac{t}{2}}\right) \end{aligned} \tag{24}$$

Thus we define,

$$\boxed{\Delta V \equiv \frac{i\omega\mu_0}{b}\int dV \;\; H_y + \frac{1}{b}\int dx \int dy \;\; \left(E_x|_{z=\frac{d}{2}} - E_x|_{z=\frac{t}{2}}\right)} \tag{25}$$

Now we assumed the CSRR metal is a PEC. Thus, we require no resistance or conductance, and so *Z and Y are purely imaginary.* To ensure our calculations reflect a lossless metal, we make the following changes.

$$\boxed{\begin{aligned} Z &\approx -\frac{i}{\Delta x}\mathrm{Im}\left[\frac{\Delta V/i}{I}\right] \\ Y &\approx -\frac{i}{\Delta x}\mathrm{Im}\left[\frac{\Delta I/i}{V}\right]. \end{aligned}} \tag{26}$$

Z and Y Derivation using Asymmetric Circuit

The CSRR pattern is technically asymmetric about the x-axis. Thus, we can also model the CSRR MTM as a 1D TL using an asymmetric circuit (See Fig. 10).

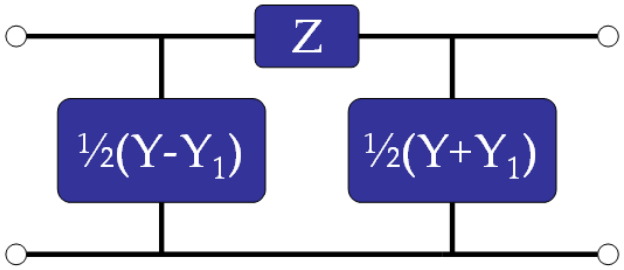

Figure 10: The unit cell of a 1D asymmetric circuit.

The transmission matrix for the circuit in Fig. 10 is given by,

$$\begin{bmatrix} A & B \\ C & D \end{bmatrix} = \begin{bmatrix} 1+\frac{1}{2}Z\left(Y+Y_1\right) & Z \\ Y+\frac{1}{4}Z\left(Y^2-Y_1^2\right) & 1+\frac{1}{2}Z\left(Y-Y_1\right) \end{bmatrix}. \tag{27}$$

To find the dispersion relation and how V & I relate to Z & Y, we setup

$$\frac{1}{AD-BC}\begin{bmatrix} D & -B \\ -C & A \end{bmatrix}\begin{bmatrix} V_{in} \\ I_{in} \end{bmatrix} = e^{i\phi_x}\begin{bmatrix} V_{in} \\ I_{in} \end{bmatrix}, \tag{28}$$

which can be manipulated to show,

$$\cos(\phi_x) = 1+\frac{ZY}{2}, \tag{29}$$

and,

$$\begin{aligned} 0 &= \left(\cos(\phi_x) - Z\frac{Y_1}{2} - e^{i\phi_x}\right)V - ZI \\ 0 &= -Y\left(1+\frac{\cos(\phi_x)-1}{2} - Z\frac{Y_1^2}{4Y}\right)V + \left(\cos(\phi_x) + Z\frac{Y_1}{2} - e^{i\phi_x}\right)I. \end{aligned} \tag{30}$$

For fixed ϕ_x and Y_1, the solutions to Eqs. (30) are,

$$\boxed{\begin{aligned} Z = & -i \quad \frac{2Z_{in}\sin(\phi_x)}{(2+Y_1Z_{in})} \\ \\ Y = & -i \quad \frac{\tan(\frac{\phi_x}{2})\,(2+Y_1Z_{in})}{Z_{in}}, \end{aligned}} \tag{31}$$

where,

$$Z_{in} = \frac{V}{I}. \tag{32}$$

Both Z and Y have the term,

$$\frac{(2+Y_1Z_{in})}{Z_{in}}.$$

To make Z and Y lossless, we require,

$$\begin{aligned} \mathrm{Im}\left[\frac{2+Y_1Z_{in}}{Z_{in}}\right] = & \quad 0 \\ \Rightarrow \mathrm{Im}\left[Y_1\right] = & -2\ \mathrm{Im}\left[\frac{1}{Z_{in}}\right]. \end{aligned} \tag{33}$$

Since there is no reason a priori for Y_1 to be lossy, we define,

$$\boxed{Y_1 \equiv \ -2i \quad \mathrm{Im}\left[\frac{1}{Z_{in}}\right].} \tag{34}$$

We now simplify expressions, and substitute them in the Eqs. (31):

$$\begin{aligned} Y_1 = & \ -2i \quad \mathrm{Im}\left[\frac{1}{Z_{in}}\right] \\ = & \frac{Z_{in}-\bar{Z}_{in}}{|Z_{in}|^2}. \end{aligned} \tag{35}$$

Then using $Z_{in} = |Z_{in}|\, e^{i\Delta}$,

$$\begin{aligned} 2+Y_1Z_{in} &= 2+\frac{Z_{in}^2-|Z_{in}|^2}{|Z_{in}|^2} \\ &= 2+\left(e^{2i\Delta}-1\right) \\ &= 2e^{i\Delta}\cos\left(\Delta\right). \end{aligned} \tag{36}$$

Thus,

$$\begin{aligned} \frac{2+Y_1Z_{in}}{Z_{in}} &= \frac{2e^{i\Delta}\cos\left(\Delta\right)}{|Z_{in}|\,e^{i\Delta}} \\ \\ &= 2\ \frac{|I|\cos\left(\Delta\right)}{|V|}. \end{aligned} \tag{37}$$

Substituting this term back into Eqs. (31), we have,

$$\boxed{\begin{aligned} Z = & -i \quad \frac{\sin(\phi_x)\,|V|}{|I|\cos(\Delta)} \\ \\ Y = & -2i\tan\left(\frac{\phi_x}{2}\right) \quad \frac{|I|\cos(\Delta)}{|V|}. \end{aligned}} \tag{38}$$

Note Eqs. (38) only compute Z and Y in terms of V and I, whereas Eqs. (26) use V, I, ΔV, and ΔI. Because ΔV and ΔI are distinct calculations from V and I, Eqs. (26) can be thought of as having more 'field information.' We can manipulate Eqs.(38) to also incorporate ΔV and ΔI. Assuming $|\phi_x| << 1$ is the simplest assumption:

$$\boxed{\begin{aligned} Z = & -\frac{[i\phi_x\,|V|]}{|I|\cos(\Delta)} \\ \\ = & -\frac{\Delta V}{|I|\cos(\Delta)} \\ \\ Y = & -\frac{[i\phi_x\,|I|]\cos(\Delta)}{|V|} \\ = & -\frac{\Delta I\cos(\Delta)}{|V|}. \end{aligned}} \tag{39}$$

Dr. Shapiro used Eqs. (39).

For the symmetric circuit, $\Delta U \leftrightarrow \left(e^{-i\frac{\phi_x}{2}} - e^{i\frac{\phi_x}{2}}\right)U = -2i\sin\left(\frac{\phi_x}{2}\right)U$, where U is either V or I. Terms equating to $-2i\sin\left(\frac{\phi_x}{2}\right)U$ were defined as ΔU. We now do the same for the asymmetric circuit. By expanding $\sin(\phi_x)$ and $\tan\left(\frac{\phi_x}{2}\right)$ in terms of $-2i\sin\left(\frac{\phi_x}{2}\right)$, we have,

$$\boxed{\begin{aligned} Y = & \frac{-\cos(\Delta)\left[-2i\sin\left(\frac{\phi_x}{2}\right)|I|\right]}{\cos\left(\frac{\phi_x}{2}\right)|V|} \\ \\ \approx & \frac{i}{\cos\left(\frac{\phi_x}{2}\right)}\,\mathrm{Re}\left[\frac{\Delta I/i}{V}\right] \\ \\ = & \frac{i}{\cos\left(\frac{\phi_x}{2}\right)}\,\mathrm{Re}\left[\frac{\omega\epsilon_0\int dx\ \int dy\ \ E_z|_{z=\frac{t}{2}}}{e^{-i\frac{\phi_x}{2}}\frac{1}{b}\int dy\int dz\ \ E_z|_{x=-\frac{b}{2}}}\right], \end{aligned}} \tag{40}$$

and,

$$
\begin{aligned}
Z = & \cos\left(\frac{\phi_x}{2}\right) \frac{\left[-2i\sin\left(\frac{\phi_x}{2}\right)|V|\right]}{|I|\cos(\Delta)} \\
& \approx i\cos\left(\frac{\phi_x}{2}\right) \ \mathrm{Re}\left[\frac{\Delta V/i}{I}\right] \\
& = i\cos\left(\frac{\phi_x}{2}\right) \ \mathrm{Re}\left[\frac{\frac{\omega\mu_0}{b}\int dV \ H_y - \frac{i}{b}\int dx \int dy \ \left(E_x|_{z=\frac{d}{2}} - E_x|_{z=\frac{t}{2}}\right)}{e^{-i\frac{\phi_x}{2}}\int dy \ \ H_y|_{x=-\frac{b}{2},\ z=\frac{t}{2}}}\right].
\end{aligned}
\tag{41}
$$

Deriving the Electron Beam-CSRR MTM Equations

Now we derive the equations used to simulate the interaction between an electron beam and the CSRR MTM. We model an electron beam as a non-relativistic, cold plasma. Let $\mathbf{v}$ be the velocity vector for the beam. The force on the beam by an electricmagnetic field is derived from the Vlasov equation[11]:

$$
mn\left[\frac{\partial \mathbf{v}}{\partial t} + \mathbf{v}\cdot\nabla\mathbf{v}\right] = -\nabla\cdot\tilde{\mathbf{P}} + qn\mathbf{E} + qn\mathbf{v}\times\mathbf{B}, \tag{42}
$$

where m is particle mass, n is the plasma density, $\tilde{\mathbf{P}}$ is the pressure tensor, and q is the particle charge.

We assume $\nabla\cdot\tilde{\mathbf{P}} \approx 0$ and $\mathbf{E} >> \mathbf{v}\times\mathbf{B}$. Since our applications are one dimensional, we treat $\mathbf{v}$ as a traveling wave in the x-direction, with frequency ω, wavenumber k_x, and phase velocity v_b:

$$
\frac{\partial \mathbf{v}}{\partial t} + \mathbf{v}\cdot\nabla\mathbf{v} \approx i\mathbf{v}\left(\omega - v_b k_x\right). \tag{43}
$$

Then Eqs. (42) and (43) implies,

$$
\mathbf{v} = \frac{ie}{m_e\left(\omega - v_b k_x\right)} E_x \hat{x}. \tag{44}
$$

For plasma, the effective current density $\mathbf{J}$ is,

$$
\begin{aligned}
\mathbf{J} = & -ne\mathbf{v} \\
& \Downarrow \\
J_x = & -\frac{i\epsilon_0\omega_p^2}{(\omega - v_b k_x)} E_x,
\end{aligned}
\tag{45}
$$

where,

$$
\omega_p^2 = \frac{ne^2}{m_e\epsilon_0} \tag{46}
$$

Lastly, we assume the electric field oscillates at frequency $(\omega - v_b k_x)$. Via Maxwell's equations and Eqs. (45),

$$\begin{aligned}(\nabla \times \mathbf{H})_x &= J_x + \frac{\partial E_x}{\partial t} \\ &= i\epsilon_0 E_x \left[1 - \frac{\omega_p^2}{(\omega - v_b k_x)^2}\right]\end{aligned} \tag{47}$$

Since the plasma oscillates only in the x-direction and is otherwise isotropic, Eqs. (47) show the x-component of the relative permittivity tensor is,

$$\boxed{\epsilon_{xx} = 1 - \frac{\omega_p^2}{(\omega - v_b k_x)^2},} \tag{48}$$

where $\epsilon_{yy} = \epsilon_{zz} = 1$.

Computationally, modeling a non-trivial polarization density is easier than modeling an electron beam. Polarization density $\mathbf{P}$ relates to $\mathbf{E}$ by,

$$\mathbf{P} = \epsilon_0 \chi_e \mathbf{E}, \tag{49}$$

where χ_e is the electric susceptibility of the material, and $\epsilon_r \equiv 1 + \chi_e = \frac{\epsilon}{\epsilon_0}$. Thus, $\mathbf{P} = \epsilon_0 (\epsilon_r - 1)\mathbf{E}$, and by Eq. (48),

$$\boxed{P_x = -\epsilon_0 \frac{\omega_p^2}{(\omega - v_b k_x)^2} E_x.} \tag{50}$$

To simulate both the CSRR MTM and the electron beam, we couple the electric field and polarization density using Eqs. (11) and (50). Note that we set $\mathbf{J} = 0$ for Eq. (11), since it is modeled by P_x. COMSOL then solves this weak form system simultaneously.

Results

Figure 11 shows the dispersion relation with varying kx phase advance. We set ky to 0°, and the vertical boundaries as either PEC or PMC. This dispersion curve agreed quantitatively with Dr. Shapiro's simulations, which were calculated on HFSS. We found six fundamental modes: 1 TEM, 1 TE, and 4 TM modes. The accelerating mode is TM, and has a negative group velocity, as seen in Fig. 12. The accelerating mode is also a negative index mode (NIM), which is more quantitatively discussed below. Figure 13 shows the type of each mode. For clarity, two TM modes ($\nu = 6.1$ GHz and $\nu = 0$ GHz at $kx = 0°$) were removed from Fig. 13. In the analysis below, we refer to the TM mode starting at 8 GHz (green curve) as the positive index mode (PIM).

Figure 14a shows the electric field at the midplane (halfway between CSRR sheets). This $\mathbf{E}$ field is longitudinal and linearly varies from -230 to -800 V/m (See Fig. 15). In addition, the Lorentz field of the accelerating mode is focusing, as shown in Fig. 14b. Although one slice is shown in Fig. 14b, focusing is seen for all xz-slices within 2 mm of the midplane. The electric field is immensely large in the CSRR gaps (See Fig. 16), and is on the order of $\pm 10^4$ V/m. The CSRR behaves like a system of capacitors at its surface.

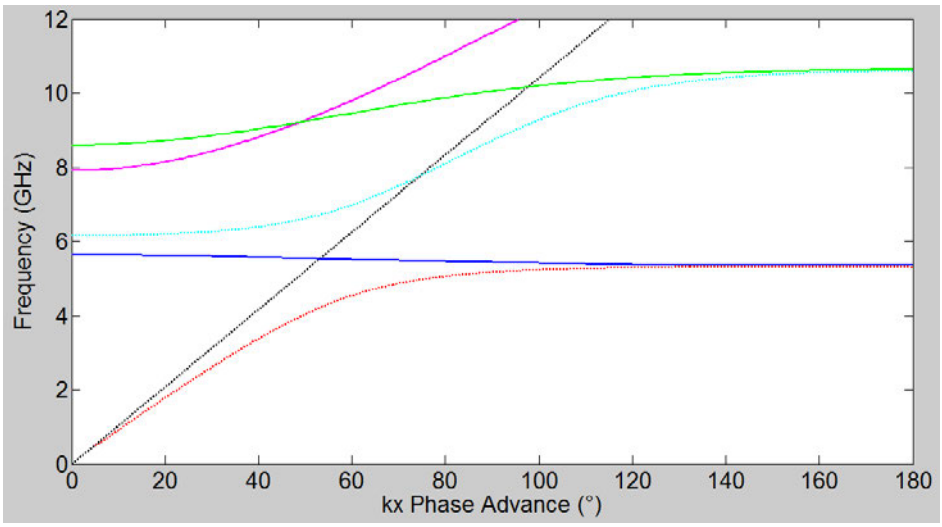

Figure 11: Dispersion relation with varying kx phase advance ($ky = 0°$). Vertical boundaries are either PEC(dashed) or PMC(solid).

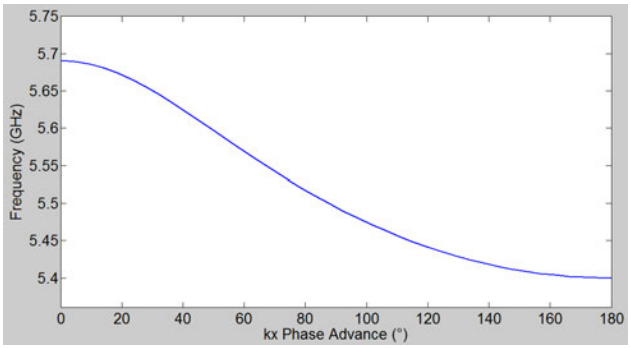

Figure 12: Dispersion for the accelerating mode

Figure 17 shows the calculated surface currents associated with the PIM and NIM. For the NIM, current mostly flows from inner metal tab toward the positive x-edge. Because of the opposite charges on the positive and negative x-edges, current appears to propagate in the x-direction. In comparison, the PIM has current flowing toward the inner tab from both the positive and negative x-edges. These characteristic current profiles are also reflected in the planar **E** fields shown in Fig. 16. The NIM's planar **E** field appears radial, whereas the PIM has opposing **E** fields in the gaps.

Figure 18 compares $\frac{|k\times\langle E\rangle|}{|k\cdot\langle E\rangle|}$ with varying kx and ky phase advance, where $\langle\mathbf{E}\rangle$ is the average phase-subtracted **E** field along the midplane for the NIM. Values of $\frac{|k\times\langle E\rangle|}{|k\cdot\langle E\rangle|}$ greater than 1 represent kx and ky values which no longer yield the accelerating properties of the NIM. Hence, Fig. 18 shows that acceleration occurs for phase advances, $(kx, ky) = (60° - 100°, 0° - 60°)$.

Figure 19 shows the dispersion of the NIM for varying kx and kz phase advances. As kz increases from zero, we see an avoided crossing: the NIM and TEM mode split into fast and slow waves. The avoided crossing implies that an electron beam can hybridize with the NIM, which permits energy exchange between them. The yellow dot in Fig. 19 represents an electromagnetic instability which occurs when an electron beam with $v_b = 0.8\ c$ propagates through the waveguide. This electric coupling is the theoretical mechanism which allows for particle acceleration and generating radiation. By using Eqs. (11) and (50), we simulated how the beam and NIM interact. With

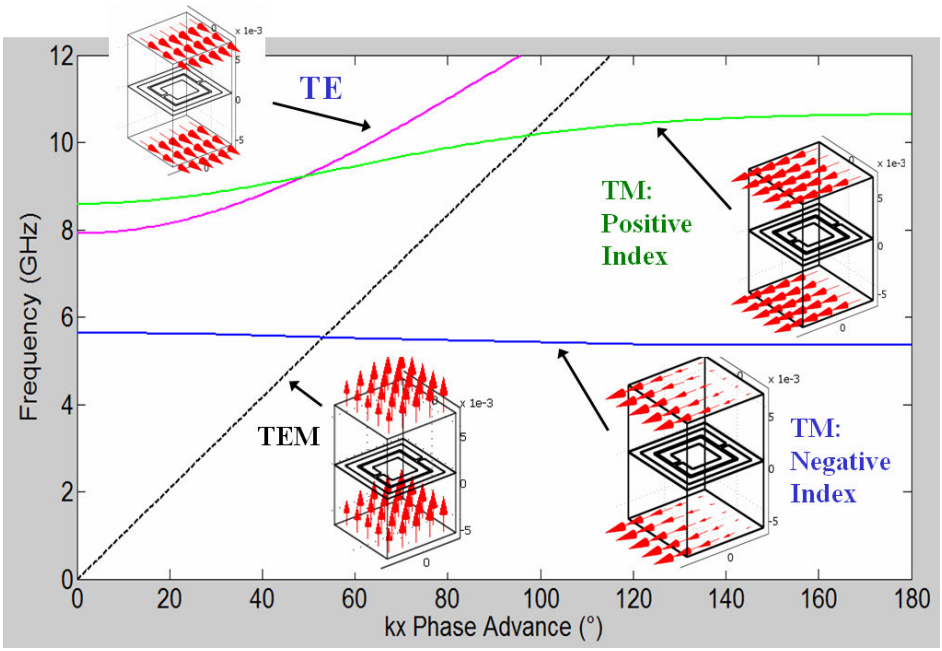

Figure 13: Comparing modes of the CSRR MTM[12]

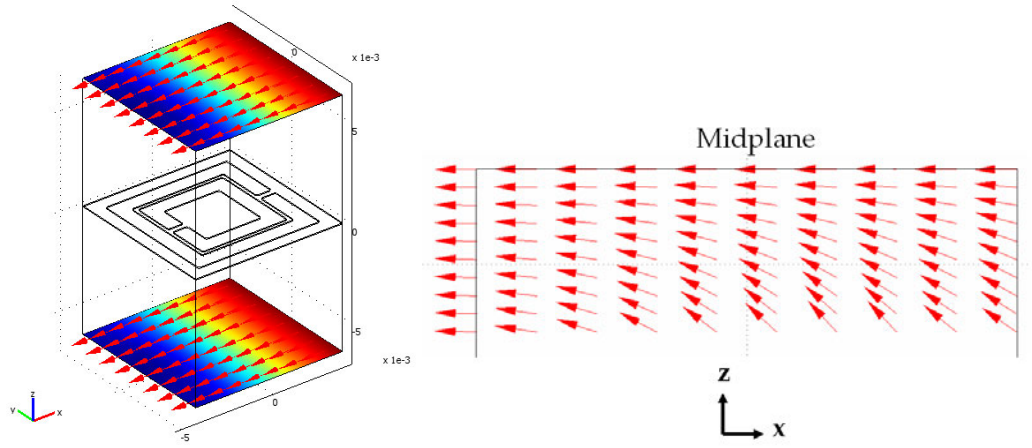

(a) Longitudinal **E** field of the accelerating mode

(b) Focusing Lorentz field of the accelerating mode

Figure 14: Properties of the accelerating mode

the help of Drs. Simeon Trendafilov (in the Shvets group) and Yaroslav Urzhumov (at Duke and COMSOL), we showed the NIM-beam model supports electron bunching (See Fig. 21), which demonstrates the plausilibity of our applications.

Using impedance boundary conditions along the CSRR metal sheets, we showed the losses for the CSRR MTM are small (See Fig. 20). We used the Drude parameters for copper[12]. The losses do not vary much, and are on average 120 MHz (2% of 5.5 GHz). Because MTMs depend on surface currents, lossy materials can hinder their practical realization. Thus, the CSRR is an efficient MTM, because of its small losses.

Lastly, we calculated the effective μ and ϵ via Eleftheriades' method. Figure 22 shows Z and Y computed from Eqs. (26). Both Z and Y are negative, which means the NIM indeed has a

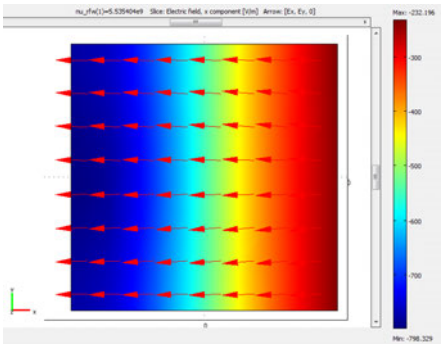

Figure 15: **E** field slice of accelerating mode at midplane

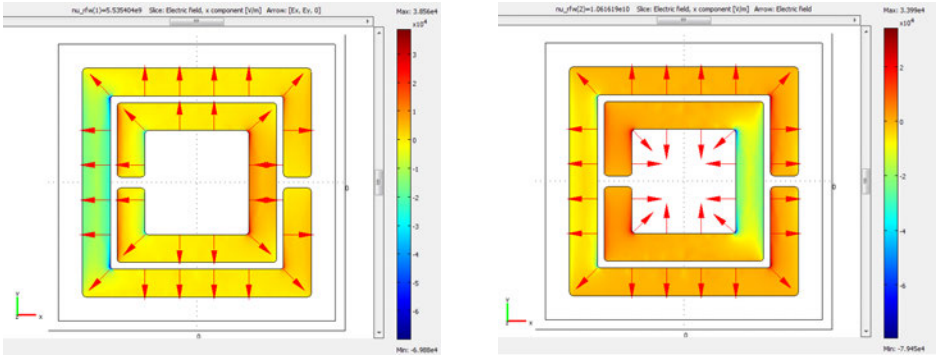

(a) Negative Index Mode (b) Positive Index Mode

Figure 16: **E** field at $z = 0$ mm. Arrows represent planar **E** field, and color data shows E_x.

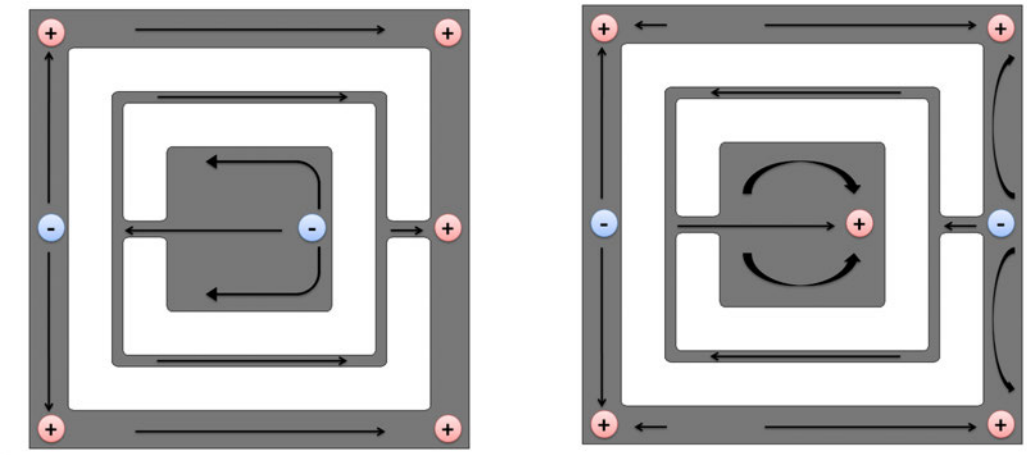

(a) Current profile for the accelerating mode (b) Current profile for the positive index mode

Figure 17: Current Profiles – red and blue circles represent net positive and negative charges, resp.

negative refractive index. However, both Z and Y are 0 at $kx = 0°$, which means $\omega = 0$. Thus, the symmetric circuit yields non-physical results.

Dr. Shapiro suggested using the asymmetric circuit, and provided Eqs. (39). Figures 23 and 24 show our calculations of Eqs. (39). For the NIM, Y is 0 at $kx = 0°$, and Z is non-zero. For the PIM, however, both Z and Y are again zero at $kx = 0°$. Dr. Shapiro reported $Z = 0$ and $Y \neq 0$

for the PIM at $kx = 0°$, so our models do not agree. We have explored why this might be true, and have been unable to account for the deviation.

In an attempt to correct this problem, we solved for Z using Eq. (41), and for Y using Eq. (29) (See Figs. 25 and 26). Y is non-zero at $kx = 0°$ for the NIM and PIM. Also, Y diverges for large kx, which reflects the expected ϵ resonance for the CSRR. However, we anticipated $Y = 0$ and $Z \neq 0$ for the NIM at $kx = 0°$. Thus, Eqs. (41) and (29) do not give reasonable Z and Y results either.

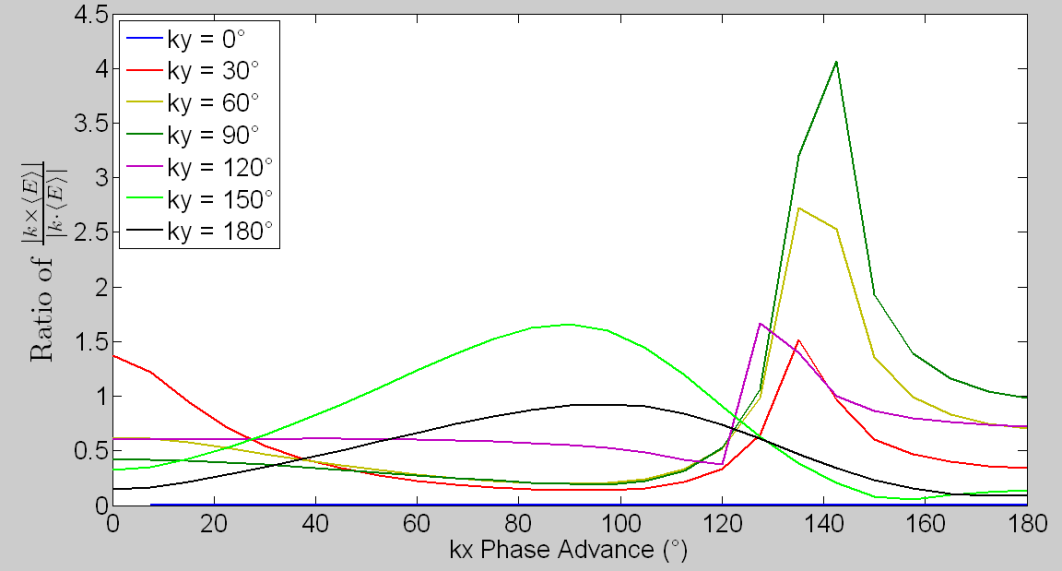

Figure 18: Comparing $\frac{|k\times\langle E\rangle|}{|k\cdot\langle E\rangle|}$ with varying kx phase advance for fixed ky for the negative index mode

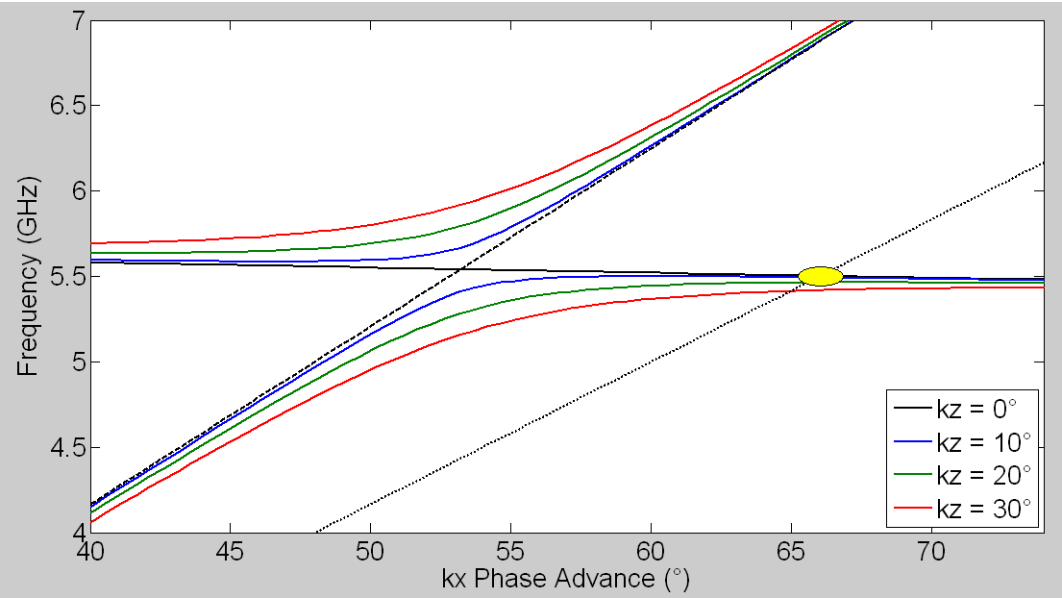

Figure 19: Dispersion relation with varying kx and kz phase advance ($ky = 0°$). The dashed line to the left is the light line, $\omega = c\ k_x$, and that to the right represents an electron beam with $v_b = 0.8\ c$.

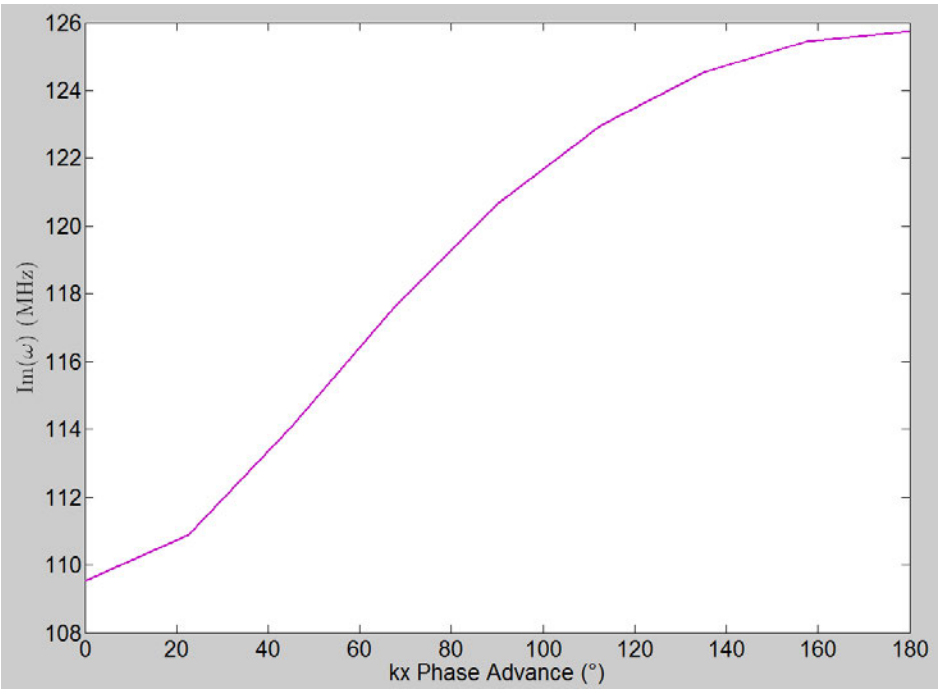

Figure 20: Calculated losses using impedance boundary conditions along the CSRR metal sheets.

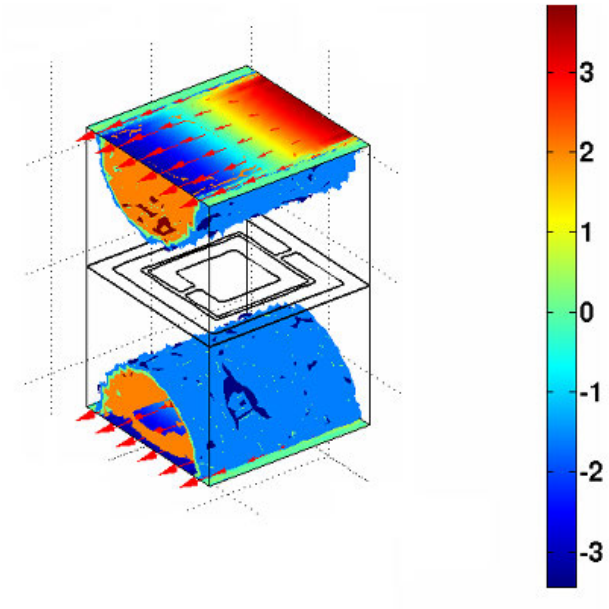

Figure 21: Simulated electron bunching occurs when the accelerating mode interacts with an electron beam[13]. Color shows electron density, and arrows show electric field.

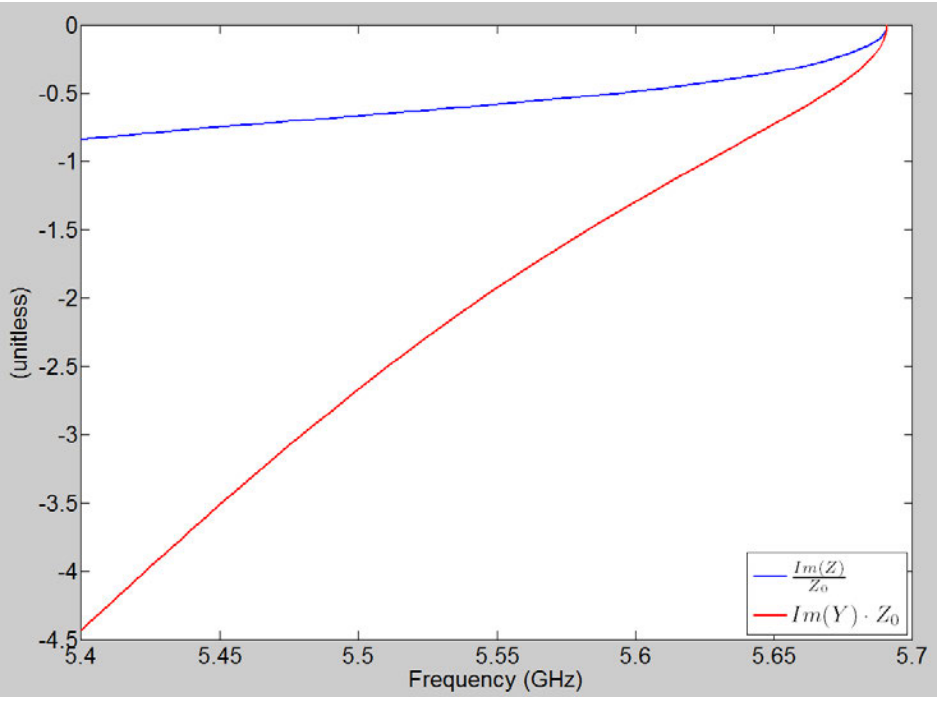

Figure 22: Calculated Z and Y for the accelerating mode using Eqs. (26).

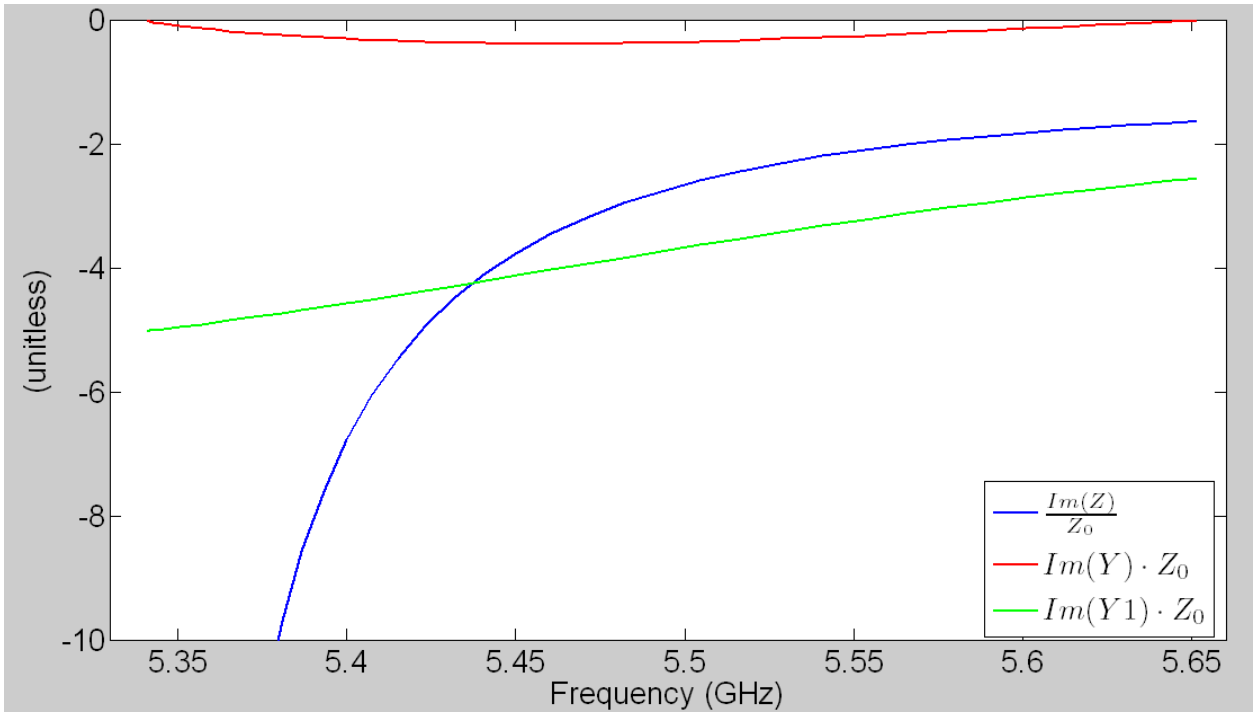

Figure 23: Calculated Z and Y for the accelerating mode using Eqs. (39), *i.e.*, Dr. Shapiro's equations.

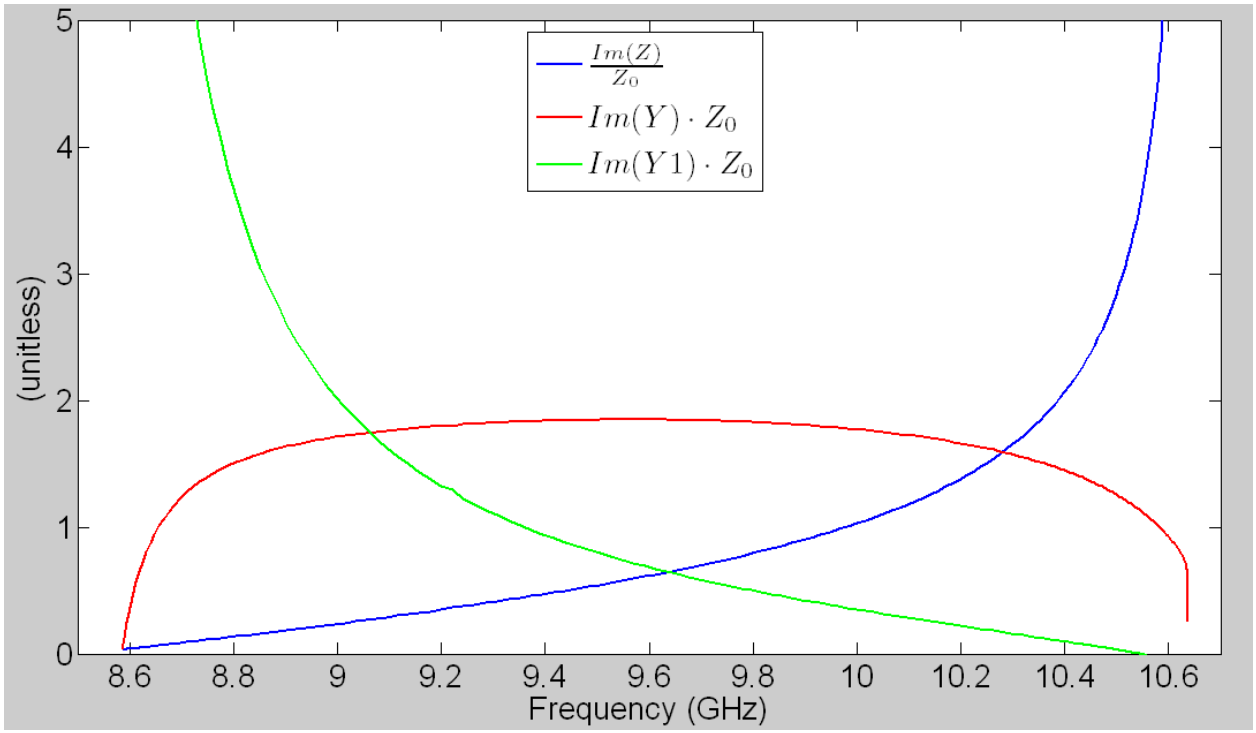

Figure 24: Calculated Z and Y for the positive index, TM mode using Eqs. (39), *i.e.*, Dr. Shapiro's equations.

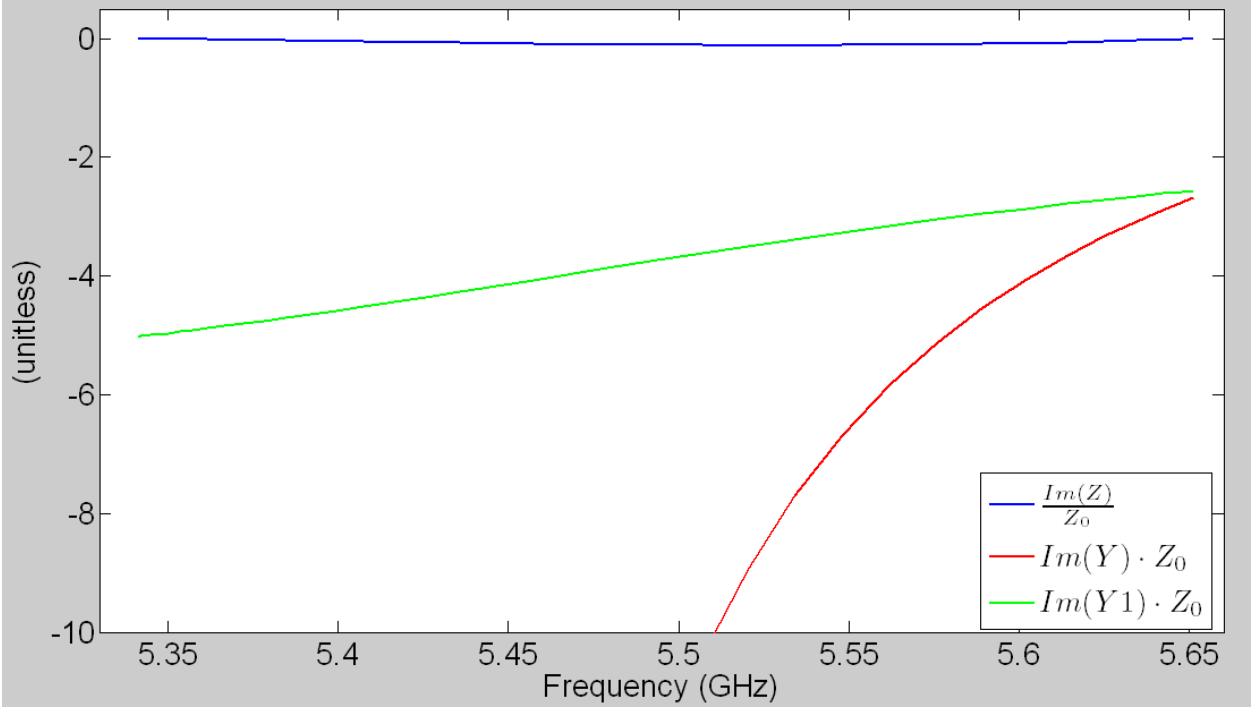

Figure 25: Calculated Z and Y for the accelerating mode using Eqs. (41) and (29).

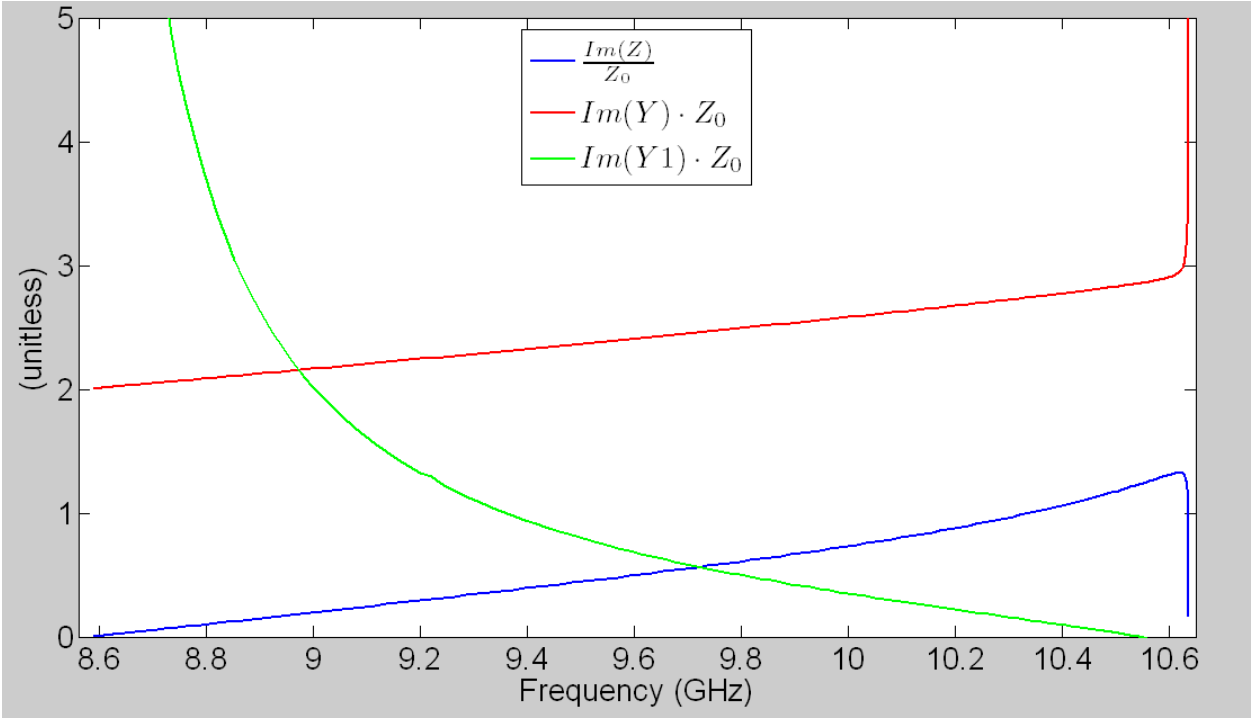

Figure 26: Calculated Z and Y for the positive index, TM mode using Eqs. (41) and (29).

Conclusion

We have motivated the application of CSRRs toward particle acceleration and generating radiation. Our FEM simulations confirmed the CSRR forms a waveguide, which has an accelerating mode characterized by backwards wave propagation. The accelerating mode has a longitudinal electric field, which can hybridize with an electron beam to exchange energy. The CSRR has small losses, and can reasonably be modeled as an ideal conductor. Although our transmission line models do not have every desired property, they do confirm that the accelerating mode has a negative refractive index, and so the CSRR composes a metamaterial. To accurately model the CSRR MTM as a transmission line requires further work.

References

1. Veselago, Victor. "The electrodynamics of substances with simultaneously negative values of epsilon and mu." Physics-Uspekhi. 10.4 (1968): 509-514. Print.

2. Shickley, Donovan. North Carolina State University. N.p., 20 Apr 2009. Web. 7 May 2010. http://www4.ncsu.edu/∼rsmith/DonovanAMGSSBeamer.pdf.

3. Pendry, JB, AJ Holden, DJ Robbins, and WJ Stewart. "Magnetism from Conductors, and Enhanced Non-Linear Phenomena." IEEE Transactions on Microwave Theory and Techniques. 47.11 (1999): 2075 - 2084 . Print.

4. Smith, DR, WJ Padilla, DC Vier, SC Nemat-Nasser, S Schultz. "Composite Medium with Simultaneously Negative Permeability and Permittivity." Physical Review Letters. 84.18 (2000): 4184-4187. Print.

5. Shamonina, E. "Slow waves in magnetic metamaterials: history, fundamentals and applications." Physica Status Solidi. 245.8 (2008): 1471-1482. Print.

6. Eleftheriades, GV, AK Iyer, and PC Kremer. "Planar Negative Refractive Index Media Using Periodically LC Loaded Transmission Lines." IEEE Transactions on Microwave Theory and Techniques. 50.12 (2002): 2702-2712. Print.

7. Jackson, John. Classical Electrodynamics. 3rd. Wiley, 1999. 488-490. Print.

8. Bonache, J, M Gil, I Gil, J Garcia-Garcia, and F Martin. "On the Electrical Characteristics of Complementary Metamaterial Resonators." IEEE Microwave and Wireless components letters. 16.10 (2006): 543-545. Print.

9. Shapiro, MA, JR Sirigiri, RJ Temkin, and G Shvets. "Metamaterial-based linear accelerator structure." Particle Accelerator Conference 2009. Vancouver, BC, Canada, 2009. Web.

10. Jin, Jianming. The Finite Element Method in Electromagnetics. 2nd ed. United States: Wiley, 2002. 186. Print.

11. Kruer, WL. The Physics of Laser Plasma Interactions. 1st ed. United States: Addison-Wesley, Inc., 1988. 10. Print.

12. Zeman, EJ, and GC Schatz. "An accurate electromagnetic theory study of surface enhancement factors for silver, gold, copper, lithium, sodium, aluminum, gallium, indium, zinc, and cadmium." Journal of Physical. 91.3 (1987): 634643. Print.

13. Shvets, G. “Homogenization of beam-driven and passive metamaterials.” AFOSR Workshop on High-Power Microwave Metamaterials. Air Force. Cambridge, MA. 6-7 Apr 2010. Presentation.